Investigation of Inter-Ion Interactions in *N,N,N',N'*-Tetramethylethylenediammonium Dithiocyanate via Experimental and Theoretical Charge Density Studies

Parthapratim Munshi,[†] Elinor Cameron,[‡] Tayur N. Guru Row,*[,†] Joseph D. Ferrara,[§] and T. Stanley Cameron*[,‡]

Solid State and Structural Chemistry Unit, Indian Institute of Science, Bangalore 560012, India, Department of Chemistry, Dalhousie University, Halifax, Nova Scotia B3H 4J3, Canada, Rigaku Americas Corp, 9009 New Trails Drive, The Woodlands, Texas 77381-5208

Received: December 13, 2006; In Final Form: May 1, 2007

The crystal structure of the *N,N,N′,N′*-tetramethylethylenediammonium dithiocyanate salt has been examined by experimental charge density studies from high-resolution X-ray diffraction data. The corresponding results are compared with multipole refinements, using theoretical structure factors obtained from a periodic density functional theory calculation at the B3LYP level with a 6-31G** basis set. The salt crystallizes in space group $P\bar{1}$ and contains only a single ion pair with an inversion center in the cation. The salt has thus one unique classical $N^+-H\cdots(NCS)^-$ hydrogen bond but also has six other weaker interactions: four C−H···S, one C−H···N, and one C−H···C_π. The nature of all these interactions has been examined topologically using Bader's quantum theory of "atoms in molecules" and all eight of the Koch−Popelier criteria. The experimental and theoretical approaches agree well and both show that the inter-ion interactions, even in this simplest of systems, play an integrated and complex role in the packing of the ions in the crystal. Electrostatic potential maps are derived from experimental charge densities. This is the first time such a system has been examined in detail by these methods.

Introduction

While studies of inter-ionic interactions in the solid state have been the subject of recent interest,[1] reports related to charge density analysis on such systems are scarce in the literature.[1−6] In such charge density analysis, however, the information carried by the electronic charge density distribution in crystals can be used to characterize and examine all the interactions, even the weak ones, in a crystal. The study of interaction between protonated cations and anion receptors where there is choice, at the molecular level, between the formation of a hydrogen bond or a complete proton transfer,[7] $B-H^+\cdots A^-$ as compared with B and HA, is also of considerable recent interest in medicine, environmental biology, and food sciences. The determination of detailed charge densities of organic, organometallic, inorganic, ionic, metallic, and mineral crystalline systems from X-ray diffraction data is now a mature and highly productive field and one of the most dynamic areas of modern X-ray crystallography.[8] Moreover, the interactions, the design element of crystal engineering,[9] can be visualized via electrostatic potential maps, where the information is derived from the charge densities.[8a,10] High-resolution ($d_{min} \approx 0.5$ Å) X-ray diffraction data at low temperatures can be used for the accurate experimental measurement and analysis of charge density distributions.[8a,11,12] The usual approach for this purpose is the Hansen and Coppens formalism,[13] which accommodates populations in core and valence and expands the atomic density as follows

$$\rho_{at}(\mathbf{r}) = P_c\rho_{core}(\mathbf{r}) + P_v\kappa^3\rho_{valence}(\kappa\mathbf{r}) + \sum_{l=0}^{l_{max}} \kappa'^3 R_l(\kappa'\mathbf{r}) \sum_{m=0}^{l} P_{lm\pm} d_{lm\pm}(\vartheta,\varphi)$$

This model describes the spherically symmetric core and valence density (first two terms) as well as the nonspherical, multipolar distribution of valence density (last term) due to chemical bonding. The core (ρ_{core}) and spherical valence ($\rho_{valence}$) densities can be calculated from Hartree−Fock (HF) or relativistic HF atomic wave functions. The atomic functions are expressed in terms of the polar coordinates r, θ, and φ, defined on the local axes centered on each atom. The density functions, also referred to as multipoles, are the product of r-dependent radial functions and θ- and φ-dependent angular functions. The surface features, or topology, of the charge density distribution obtained from experimental or theoretical methods can be analyzed via Bader's quantum theory of "atoms in molecules" (AIM).[14] This approach provides a pathway for comparison of the experimental electron density with the theoretically derived density in terms of the topological properties of the charge density, $\rho(r)$. The topology of a scalar field, such as $\rho(r)$, which is a physical quantity, can conveniently be summarized in terms of critical points (CPs), where the first derivatives of $\rho(r)$ vanish, $\nabla\rho(r) = 0$, indicating the position of extrema (maxima, minima, or saddles) in the $\rho(r)$ at r_c. In general, the theory of AIM provides a methodology for the identification of a bond between any two atoms in a molecule in terms of CPs, called bond critical points (BCPs). For every pair of nuclei, linked via chemical bond, shared or closed shell interactions, (3, −1) type CPs, and the properties of ρ(r) at these points, provide the chemically most useful information. (The three eigenvectors of the Hessian matrix coincide with the three orthogonal principal axes of

* Authors to whom correspondence should be addressed. E-mail: stanley.cameron@dal.ca, ssctng@sscu.iisc.ernet.in.
† Indian Institute of Science.
‡ Dalhousie University.
§ Rigaku Americas Corp.

10.1021/jp068554x CCC: $37.00
Published on Web 07/21/2007

SCHEME 1 : Structural Diagram of the Title Compound

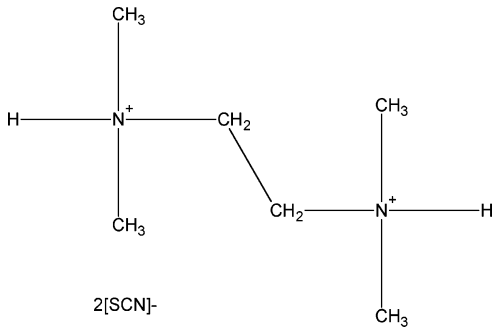

curvature of the bond. When one corresponding eigenvalue (λ_n, $n = 1-3$) is positive and the other two are negative, this indicates that the electron density at the BCP is at a minimum along one axis and a maximum along the other two axes. This is the classical "saddle point" and is denoted by (3, −1).) The line of the highest electron density linking any two atoms is referred to as the bond path (BP), and its length, which need not be the same as the interatomic vector, is referred to as the interaction line (R_{ij}). The BP passes through the BCP. The existence of a (3, −1) CP and associated BP is the topological definition of a chemical bond. A quantitative measure of the ellipticity of a bond, bond ellipticity, is defined as $\epsilon = \lambda_1/\lambda_2 - 1$, where λ_2 is the curvature of smaller magnitude. Within related sets of bonds, the bond order (and bond strength) is defined[8d] by the magnitude of the charge density at the BCP, $\rho_b(r)$. An important function of $\rho(r)$ is its second derivative, the Laplacian $\nabla^2\rho(r)$, which is a scalar quantity and is defined as the sum of the principal curvatures ($\lambda_1 + \lambda_2 + \lambda_3$). The electron densities, the Laplacian values, the interaction lines, the curvatures, and the bond ellipticities together represent the topology of the charge density distribution. The AIM approach could be used for both theoretical and experimental analyses.

Topological analysis provides the information about the existence and the nature of a bond, but it does not specify the character of the bond. To distinguish a hydrogen bond from a van der Waals interaction,[15,16] in terms of chemical concepts, Koch and Popelier (KP) have proposed eight criteria, which are based on Bader's quantum theory of AIM. If any of these eight criteria are not satisfied, the interaction concerned can be considered as a van der Waals interaction. Among the set of criteria, the fourth criterion is considered as necessary and sufficient to describe fully a hydrogen bond. The following describes the eight criteria:

(1) Topology. Confirmation of the presence of a BCP between a donor atom and an acceptor atom linked via a BP.

(2) Charge Density at the BCP. There should be significant charge density ($\rho(r_{CP})$) at the BCP. The magnitude of the charge density evaluated at the BCP is related to the overall hydrogen bond energy. The local energy density $E(r_{CP})$ of the electrons is determined by evaluating the local electronic kinetic energy density $G(r_{CP})$ and the local potential energy density $V(r_{CP})$ using the equations[14a,17]

$$G(\mathbf{r}_{CP}) = \left(\frac{3}{10}\right)(3\pi^2)^{2/3}\rho^{5/3}(\mathbf{r}_{CP}) + \left(\frac{1}{6}\right)\nabla^2\rho(\mathbf{r}_{CP})$$

$$V(\mathbf{r}_{CP}) = \left(\frac{1}{4}\right)\nabla^2\rho(\mathbf{r}_{CP}) - 2G(\mathbf{r}_{CP})$$

and

$$E(\mathbf{r}_{CP}) = G(\mathbf{r}_{CP}) + V(\mathbf{r}_{CP})$$

TABLE 1: Single-Crystal Data of *N,N,N',N'*-Tetramethylethlenediammonium Dithiocyanate at 113 K

formula	$C_8H_{18}N_4S$	space group	$P\bar{1}$
crystal size/mm	0.31 × 0.18 × 0.11	D_c/g cm^{-3}	1.238
formula weight	234.4	$F(000)$	126
crystal system	triclinic	μ/mm^{-1}	0.396
unit cell dimensions		$T_{min, max}$	0.9240, 0.9571
a/Å	5.8915(2)	$(\sin\theta/\lambda)_{max}$/Å^{-1}	1.1
b/Å	6.8875(2)	reflection nos. (unique)	5303
c/Å	8.2113(2)	R(merge)	0.0255
α/deg	73.8950(10)	$R(F)$; $R_w(F)$	0.0187; 0.0174
β/deg	79.2280(10)	S	1.69
γ/deg	85.9170(30)	N_{obs}/N_{par}	24.55
Z; V/Å^3	1; 314.41(2)	range of residuals/ e Å^{-3}	−0.158; 0.168

(3) The Laplacian of the Charge Density at the BCP. The calculated values of Laplacian, $\nabla^2\rho_b(r)$, should be positive but within a sensible range and should correlate with the interaction energy.

(4) Mutual Penetration of the Hydrogen and the Acceptor Atom. This compares the nonbonded radii of the donor hydrogen atom (r_D^0) and the acceptor atom (r_A^0) with their corresponding bonding radii, r_D and r_A. The nonbonding radius, the distance from the nucleus to an arbitrary charge contour (0.001 au), is taken to be equivalent to the gas-phase van der Waals radius of the participating atoms.[18] The bonding radius is the distance from the nucleus to the BCP. In a typical hydrogen bond, the values of $\Delta r_D = (r_D^0 - r_D) > \Delta r_A = (r_A^0 - r_A)$ and $\Delta r_D + \Delta r_A > 0$ represent positive interpenetration. If either or both of these conditions are violated, then the interaction is essentially van der Waals in nature. This condition is considered as necessary and sufficient to prove the existence of a hydrogen bond.

The remaining four criteria can be obtained from integration over the atomic basins of the participating H atoms and these calculations are computationally more expensive. These last four criteria are purely based on properties associated with the H atoms and are probably not independent criteria.

(5) Loss of Charge. The H atom loses electron density, resulting in an increased net charge on the H atom. The descreening of hydrogen-bonded protons, as observed in NMR chemical shifts, follows this phenomenon.

(6) Energetic Destabilization. The energy of the H atom is destabilized when it forms a hydrogen bond. The difference in total energy between the crystal and the bare molecule should thus be positive. This condition strongly correlates with criterion 5.

(7) Decrease in Dipolar Polarization. There should be a decrease of the dipolar polarization (magnitude of the first moment, M) of the H atom upon hydrogen bond formation. This essentially indicates the loss of nonbonding density on the H atom compared with that in the molecule without the hydrogen bond.

(8) Decrease in Volume. The integrated volume of the H atom should be depleted upon forming a hydrogen bond.

In a study of a series of organo-ethylenediammonium thiocyanate salts,[19] where the ammonium salts were examined in a sequence $-NH_3^+$, $-N(CH_3)H_2^+$, $-N(CH_3)_2H^+$, it was found that the occurrence of hydrogen bonds, such as N−H···(NCS) and $N^+-H\cdots(SCN)^-$, varies logically with the variation in the ratio of $[N-H]^+$ bonds to SCN^- anions. It was noticed that when the ratio of $[N-H]^+$ bonds to SCN^- anions was 1:1

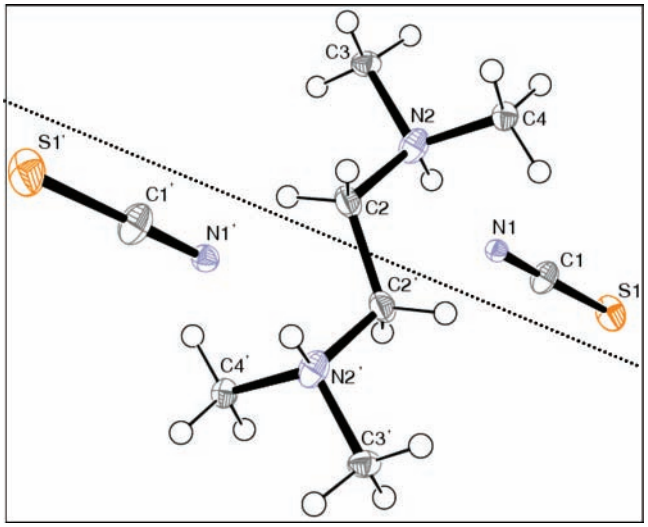

Figure 1. ORTEP view at 113 K with 50% ellipsoid probability (non-hydrogen atoms)

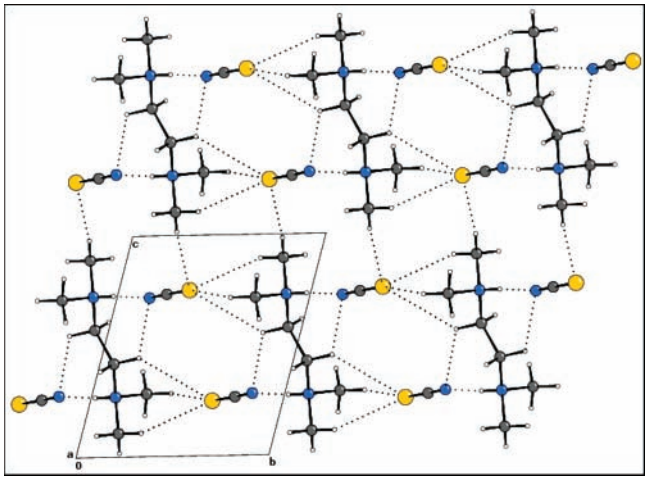

Figure 2. Packing diagram, viewed down the *a*-axis, showing the arrangement of the ionic species and the interactions associated with those ions.

(i.e., $-N(CH_3)_2H^+/SCN^-$), then an N−H···NCS hydrogen bond was formed. When the ratio developed through 1.5:1 to 2:1 ($-N(CH_3)H_2^+/SCN^-$), then bifurcated hydrogen bonds were formed but still with N−H···NCS bonding, while at higher ratios, 2.5:1 and 3:1, an N−H···SCN hydrogen bond was formed in addition to bifurcated or trifurcated N−H···NCS systems. However, in an examination of a wider variety of donor species it was noticed that the hydrogen-bonding hierarchy was not as simple as had been proposed. This was particularly true when the series was expanded to include thiocyanate salts of some of the cyclic diamines (the piperazines for example). To investigate the underlying causes behind these observations, the salt *N,N,N′,N′*-tetramethylethylenediammonium dithiocyanate [$Me_4enH_2(SCN)_2$] was chosen for investigation. This compound was selected for several reasons: First, it is the simplest of the salts having an $[N-H]^+$ to SCN^- ratio of 1:1; this produces a simple linear $N^+-H\cdots(SCN^-)$ hydrogen bond that does not interfere with any other interactions in the crystal. Second, the salt crystallizes in the centrosymmetric space group, $P\bar{1}$, with $Z = 1$, and with thus only one-half of the molecule in the asymmetric unit. This reduces the number of parameters to be refined. Finally, the crystals diffract well with Mo Kα radiation giving measurable reflection intensities within the required resolution. The SCN^- anion is a pseudo-halogen, with its basicity, at nitrogen, positioned between F^- and Cl^-. It is thus close to the boundary for the transformation from $B-H^+\cdots A^-$ to B and HA.[7] The selection of this salt for investigation also allows an examination of the $B-H^+\cdots A^-$/B and HA options at the detailed charge density level.

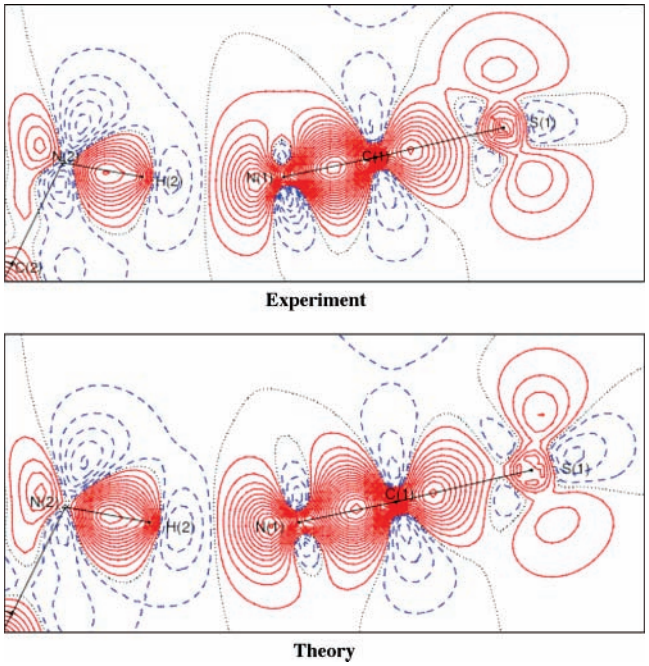

Figure 3. Static deformation density maps (experimental and theoretical). The positive (solid red lines) and negative (broken blue lines) contours start at $\pm 0.025e$ Å^{-3}, and the interval is of $\pm 0.05e$ Å^{-3}; contour at zero is shown as a black dotted line.

Here, we report the topological features of experimental and theoretical charge densities and the identification and characterization of interactions such as $N^+-H\cdots N^-$, C−H···N, C−H···S, and C−H···C_π, based on all of the eight of KP criteria[16,17] and Bader's quantum theory of AIM.[14a] This is the first full examination of the SCN^- anion since the classic study by Coppens of NaSCN and NH_4SCN nearly 30 years ago.[2,3]

Experimental Methods

The pure amine, $(CH_3)_2NCH_2CH_2N(CH_3)_2$, was treated with dilute H_2SO_4 until the resulting solution was slightly acidic. The solution was then treated with $Ba(SCN)_2$ solution (one of the unusually soluble salts of Ba), until no more precipitate of $BaSO_4$ was formed. The $BaSO_4$ was filtered off, and the resulting solution was evaporated to dryness. The compound was then dissolved in ethyl alcohol and left for crystallization. The molecular diagram of the compound is given in Scheme 1.

Single-Crystal Data Collection and Spherical Refinement. High-resolution single-crystal X-ray diffraction data were collected on an AFC8/Saturn70 CCD diffractometer using Mo Kα radiation. During the data collection, the temperature was maintained at 113.0 (3) K with a Rigaku X-Stream cooling system. A suitable crystal of reasonable size (Table 1) was mounted on the tip of a Lindeman glass. (A tube gives much more rigidity to vibrations from the gas flow than a rod of a similar diameter, and a fine needle point of Lindeman glass greatly reduces any X-ray scatter from the mounting.) When the crystal was mounted on a glass fiber, when viewed at a magnification of 100, it appeared to vibrate slightly under the cooling gas flow. This vibration was not visible at the same magnification when the crystal was remounted on top of a 1

TABLE 2: Bond Critical Points for the Covalent Bonds[a]

bonds (A−B)	ρ_b (e Å^{-3})	$-\nabla^2\rho_b$ (e Å^{-5})	d_1 (A−CP) (Å)	d_2 (CP−B) (Å)	λ_1 (e Å^{-5})	λ_2 (e Å^{-5})	λ_3 (e Å^{-5})	ϵ
S(1)−C(1)	1.53(2)	−7.92(5)	0.7448	0.8850	−6.68	−6.08	4.84	0.10
	1.51	*−7.76*	*0.7563*	*0.8790*	*−7.13*	*−6.50*	*5.87*	*0.10*
N(1)−C(1)	3.16(1)	−9.85(8)	0.7666	0.4033	−25.66	−24.82	40.63	0.03
	3.13	*−15.52*	*0.7598*	*0.4099*	*−24.23*	*−23.97*	*32.67*	*0.01*
N(2)−C(2)	1.64(1)	−9.92(3)	0.8621	0.6338	−11.24	−10.63	11.94	0.06
	1.57	*−8.02*	*0.8709*	*0.6248*	*−10.39*	*−9.88*	*12.25*	*0.05*
N(2)−C(3)	1.65(1)	−10.08(4)	0.8714	0.6199	−10.83	−10.69	11.43	0.01
	1.56	*−7.24*	*0.8685*	*0.6227*	*−10.01*	*−9.52*	*12.29*	*0.05*
N(2)−C(4)	1.62(1)	−9.19(4)	0.8625	0.6302	−10.83	−10.21	11.85	0.06
	1.58	*−7.72*	*0.8753*	*0.618*	*−10.10*	*−9.71*	*12.09*	*0.04*

[a] The values from the periodic calculation using the B3LYP/6-31G** method are given in italics.

TABLE 3: Parameters Characterizing the Intermolecular Interactions[a]

interaction	$\Delta r_D - \Delta r_A$ (Å)	$\Delta r_D + \Delta r_A$ (Å)	hydrogen bond?	R_{ij} (Å)	ρ_b (e Å^{-3})	$\nabla^2\rho_b$ (e Å^{-5})	$G(r_{CP})$ (kJ mol^{-1} b^{-3})	$V(r_{CP})$ (kJ mol^{-1} b^{-3})
H(2)−X1_N(1)	0.154	1.039	yes	1.761	0.271	3.850	105.41	−105.96
($x-1, y, z$)	*0.185*	*1.036*		*1.764*	*0.264*	*4.060*	*107.71*	*−104.84*
H(3C)−X1_S(1)	0.280	0.115	yes	2.825	0.041	0.668	13.65	−9.11
($x, y+1, z$)	*0.233*	*0.125*		*2.815*	*0.048*	*0.691*	*14.53*	*−10.24*
H(3B)-X2_S(1)	0.342	0.098	yes	2.842	0.035	0.689	13.68	−8.60
($-x+2, -y, -z$)	*0.339*	*0.097*		*2.843*	*0.038*	*0.686*	*13.80*	*−8.92*
H(2B)−X2_N(1)	−0.009	−0.033	no	2.833	0.035	0.505	10.34	−6.93
($-x+3, -y, -z+1$)	*−0.013*	*−0.037*		*2.837*	*0.033*	*0.491*	*9.98*	*−6.58*
H(4B)−X1_S(1)	0.213	−0.050	no	2.990	0.033	0.479	9.76	−6.47
($x, y+1, z$)	*0.179*	*−0.067*		*3.007*	*0.032*	*0.439*	*8.98*	*−6.00*
H(2B)−X1_S(1)	0.230	−0.142	no	3.082	0.034	0.440	9.11	−6.23
($x, y+1, z$)	*0.209*	*−0.152*		*3.092*	*0.031*	*0.421*	*8.60*	*−5.74*
H(4C)−X2_C(1)	−0.221	0.246	no	2.804	0.026	0.415	8.25	−5.20
($-x+2, -y, -z+1$)	*−0.178*	*0.240*		*2.810*	*0.025*	*0.395*	*7.84*	*−4.92*

[a] The values from the periodic calculation using the B3LYP/6-31G** method are given in italics. The symmetry codes are given below each entry of the first column.

mm capillary, which had the top sealed and then pulled to a sharp point. The data were collected with 16 scans, each covering 180° in ω at 0.5°/frame at 120 s/deg, with ($\chi = 0°$ and $\phi = 0°$, 180°; $\chi = 45°$ and $\phi = 45°$, 90°, 135°, 180°, 225°, 270°, 315°) for 2θ settings of 40° and 80°. The crystal-to-detector distance was fixed at 3.956 cm. This strategy provides completeness in the data sets up to 95% and covers all of the reflections to the observable limit with an average redundancy of 4.46 and resolution of 0.45 Å [$(\sin\theta/\lambda)_{max} = 1.1$ Å^{-1}]. The data collection was monitored and reduced with the package HKL2000.[20] Sorting, scaling, merging, and application of an empirical correction for absorption of the measured set of intensities were performed with SORTAV.[21] The structure was solved by direct methods using SHELXS97[22] and refined in the spherical atom approximation (based on F^2) using SHELXL97[22] included in the package WinGX.[23] The molecular thermal ellipsoid plots are generated using ORTEP-3.[24,25]

Multipole Refinement. Multipolar refinement of the data set was carried out with the module XDLSM incorporated in the software package XD.[26] Scattering factors were derived from the Clementi and Roetti[27] wave functions for all atoms. The function minimized in the least-squares refinement is $\sum w(|F_0|^2 - K|F_c|^2)^2$ for all reflections with $I > 3\sigma(I)$. Initially, only the scale factor was refined with all reflections. Next, the higher-order ($\sin\theta/\lambda \geq 0.8$ Å^{-1}) refinements were performed for position and anisotropic thermal parameters of the non-hydrogen atoms. The isotropic thermal parameters of the H atoms were then refined using the lower-angle data ($\sin\theta/\lambda \leq 0.8$ Å^{-1}). The positions of the H atoms in this refinement as well as in the subsequent refinements were fixed to average bond distance values obtained from reported[28] neutron diffraction studies (e.g., N−H = 1.03 Å and C−H = 1.06 Å). In the next stage of the refinements, monopole, dipole, quadrupole, octapole, and hexadecapole (only for the sulfur atom) populations (with a single κ) were released in a stepwise manner. Finally, a single κ' was refined for all non-hydrogen atoms along with the rest of the parameters (including the isotropic thermal parameters of the H atoms). This refinement indicates that the multipole density function of S atom has quite high κ' value (~1.4) and hence is quite contracted. Consequently, the κ' values of all non-hydrogen atoms were fixed to the values obtained from the multipole refinement of the theoretical structure factors. This is a well-known approach, and its advantage has already been discussed.[29] For all H atoms the multipole expansion was truncated at the $l_{max} = 1$ (dipole, bond-directed) level. For each chemically different group of non-hydrogen atoms separate κ and κ' were allowed while for H atoms; the corresponding values were fixed at 1.2. No chemical restraints were applied, and the scale factor was allowed to refine. The modules XDFFT[26] and XDFOUR[26] were used to compute the residual electron density and the dynamic deformation density and hence confirmed the refinement procedure. The module XDPROP[26] of the package XD was used for topological analysis of the charge densities.

Theoretical Calculations and Refinement. The program CRYSTAL03[30] was used to perform single-point periodic calculations based on the experimental geometry using the density functional theory (DFT) method at the B3LYP[31] level with a 6-31G** basis set.[32] This basis set has been shown to provide reliable and consistent results in studies involving intermolecular interactions.[33,34] The shrinking factors (IS1, IS2, and IS3) along the reciprocal lattice vectors were set at 4 (30 K-points in the irreducible Brillouin zone). The truncation parameters (ITOL) were set as ITOL1 = ITOL2 = ITOL3 = ITOL4 = 6 with ITOL5 = 15. For faster convergence rates the level shifter value was set at 0.5 hartree. Upon convergence on energy (~10^{-6}) the periodic wave function was obtained, and

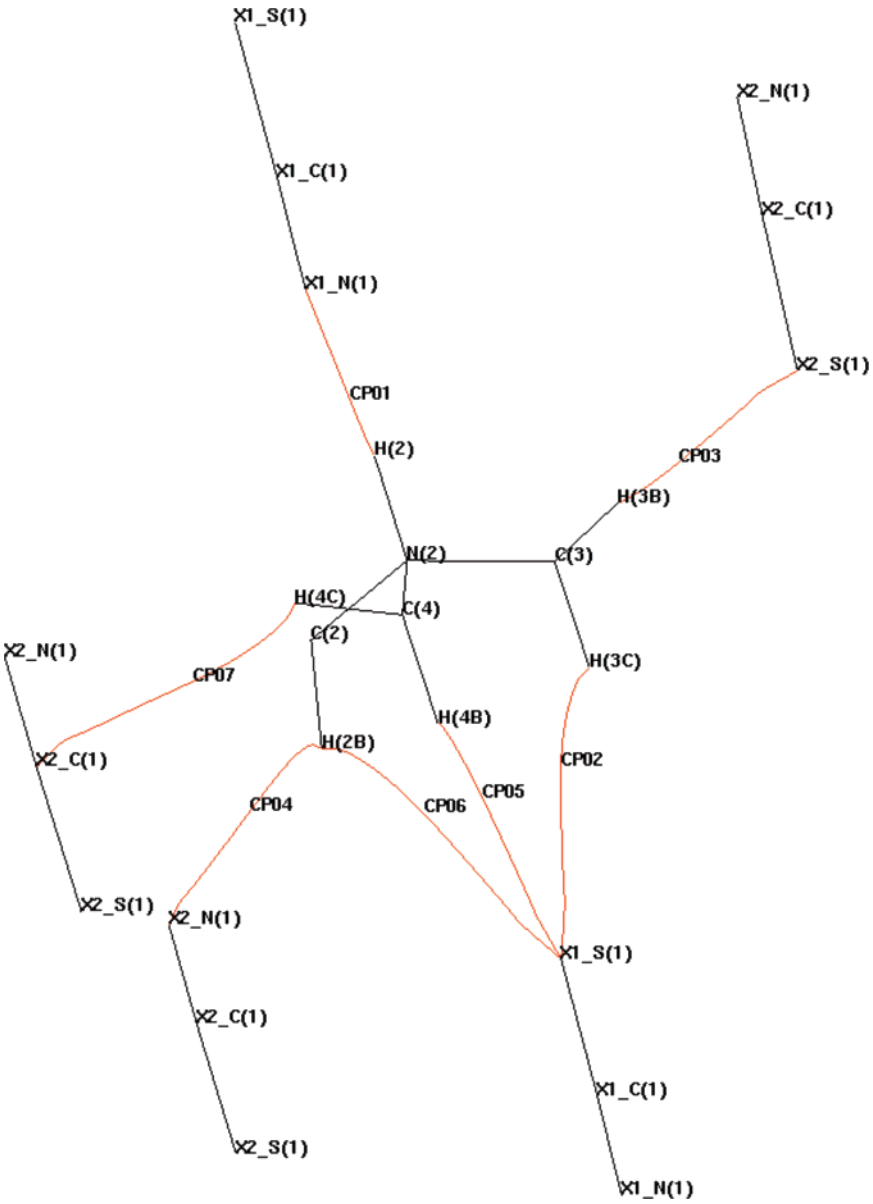

Figure 4. Bond path characters, showing the BCP locations along the $N^+-H\cdots N^-$ hydrogen bond and $C-H\cdots S$, $C-H\cdots N$, and $C-H\cdots C_\pi$ interactions in red. The symmetry codes are the same as those listed in Table 3.

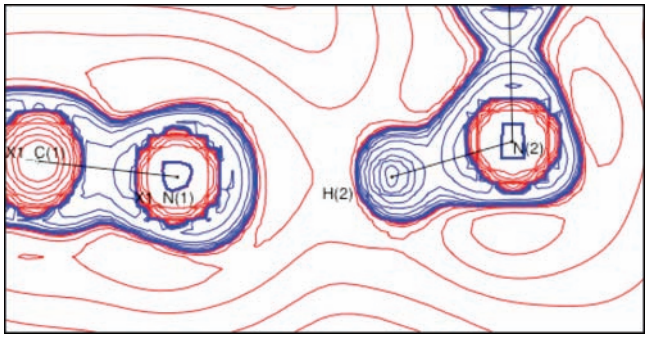

Figure 5. Laplacian $[\nabla^2\rho_b(\mathbf{r})]$ distribution of the $N^+-H\cdots N^-$ hydrogen bond, the contours drawn at logarithmic intervals in $-\nabla^2\rho_b$ eÅ^{-5} shown with blue and red lines representing the positive and negative contours, respectively.

it was used to generate the theoretical structure factors at the same resolution as the experiment, $(\sin\theta/\lambda)_{max} = 1.1$ Å^{-1}, using the option XFAC.

The multipoles, the same as those used in the refinement of the experimental structure factors, were allowed to refine, with separate κ' parameters for each non-hydrogen atom. All the theoretical reflections were included in the refinements. The module XDPROP of the package XD was used for topological analysis of the resulting electron densities via a multipole model projected through static structure factors.

Evaluation of Atomic Basin Properties. These properties include the determination of the charge, potential energy, dipolar polarization, and volume of H atoms, considering the crystal (experimental and theoretical) and the isolated ions. The module TOPXD,[35] implemented in the package XD, was used for the calculation of these properties in the crystal while the program MORPHY98[36] provided the information for the isolated ions in the gas phase. Ab initio geometry optimization and the corresponding wave functions for the isolated ions were obtained via Gaussian 98[37] using DFT at the B3LYP level with a 6-31G** basis set. Similar values of the integration variables were used to perform the calculations in evaluating the atomic basin properties in both the crystal and the gas phase. Since the calculations on the theoretical crystal were performed with DFT (B3LYP/6-31G**), the corresponding calculations in the gas phase were also performed with this method, allowing a

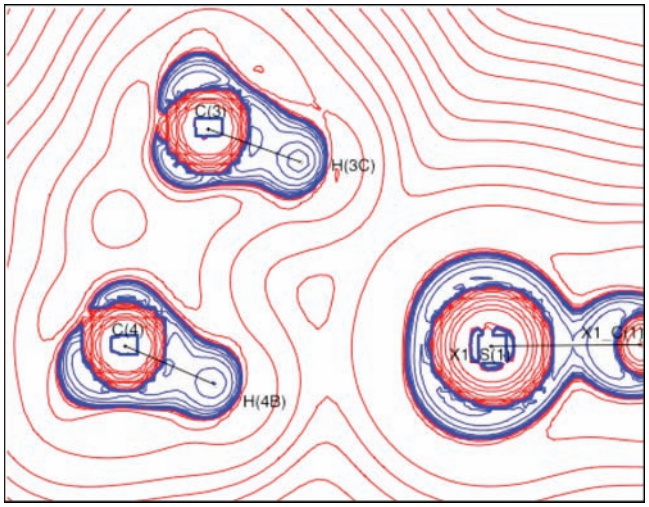

Figure 6. Laplacian $[\nabla^2\rho_b(\mathbf{r})]$ distribution of the bifurcated C−H···S interactions.

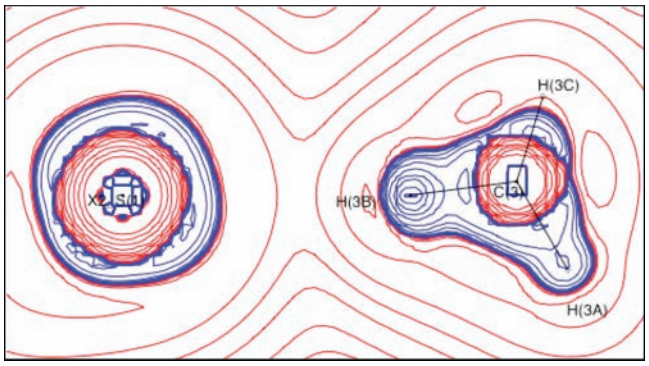

Figure 7. Laplacian $[\nabla^2\rho_b(\mathbf{r})]$ distribution of the C−H···S interaction.

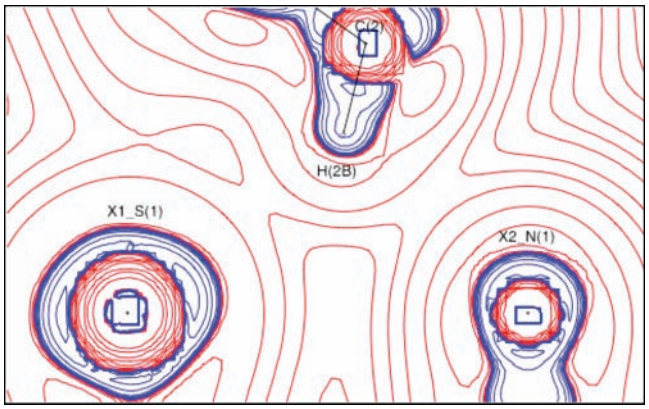

Figure 8. Laplacian $[\nabla^2\rho_b(\mathbf{r})]$ distribution of the bifurcated C−H···S and C−H···N interactions.

direct comparison of the results obtained from the isolated ions and the theoretical crystal.

Results and Discussion

This sulfur-containing ionic compound crystallizes in the triclinic system with the centrosymmetric space group, $P\bar{1}$ (no. 2). Figure 1 shows an ORTEP view of the structure, indicating the atom labeling for the complete molecule. The salt consists of one-half of the molecule in the asymmetric unit. The other half, generated by symmetry, is shown in Figure 1 below the dotted line, and the atoms of the second half are labeled accordingly. The packing diagram shown in Figure 2 illustrates the arrangement of the ionic species in the crystal. It has a

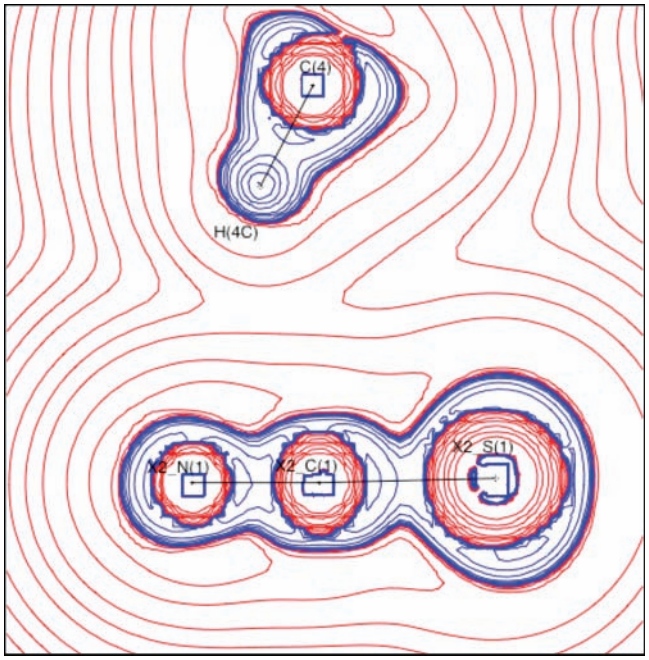

Figure 9. Laplacian $[\nabla^2\rho_b(\mathbf{r})]$ distribution of the C−H···C_π interaction and the SCN^- anion.

parallel stacking along the crystallographic *b*-axis. From geometrical analysis it is clear that the inter-ion interactions are mainly associated with the S and N atoms. The investigations of the interactions and the corresponding quantitative features associated with these interactions are examined from the charge density point of view in the later section of this article. The unit cell parameters, experimental details, and multipole refinement parameters, including the residual densities over the asymmetric unit are listed in Table 1. During the final refinement, Hirshfeld's rigid bond test[38] was applied to the covalent bonds. The maximum difference in the mean-square displacement amplitude (DMSDA) value was found to be 5×10^{-4} Å^2 for the bond N(2)−C(3), indicating that the atomic thermal vibrations have been properly accounted for. In a recent study by Dominiak and Coppens, several combinations of radial function parameters were tested to optimize the multipolar model of the valence-electron density distribution for S atoms for a number of organic molecules.[39] However, with this present structure, a trial with a suitable set [2,4,6,8] of radial function parameters[40] did not improve the model, and there was an increase of residual densities compared with the default choice of parameters [4,4,4,4] for the S atom. A feature of the multipole concept of expanding[39] the orbitals will be the introduction of tighter electron packing at and near the S atom. In this type of ionic species, the consequences will then have to be an increase in the residuals, particularly near S because of the polarizing nature of the $[SCN]^-$ species. In this case, the default choice of S atom parameters appeared to suit well mainly because of the ionic nature and the consequent directionality in the bonding region. Therefore, the standard set of radial function parameters were used to model the S atom. However, this model still resulted in relatively high residuals near the S atom. Similar observations have been noticed in several other studies on sulfur-containing compounds[5,33,41−43] where it was also seen that that the correct modeling of the charge density distribution in the vicinity of S atom appeared to be difficult.[41] However, the residuals along with the *R*-factors and the goodness of fit (GOF) values were significantly improved when the thermal motion analysis on S atom was modeled with the refinement of the third-order coefficients of a Gram−Charlier expansion, as

TABLE 4[a]

(a) Atomic Net Charges (q) of the H Atoms in the Crystal and in the Isolated Ions and Their Corresponding Differences (in au)

		q (crystal)		q (isolated)	Δq (crystal − isolated)	
interactions	atoms	experiment (E)	theory (T)	DFT	E-DFT	T-DFT
N(1)···H(2)	H(2)	0.4634	0.4834	0.3436	0.1198	*0.1398*
N(1)···H(2B)	H(2B)	0.0545	0.0963	0.0372	0.0173	*0.0591*
S(1)···H(2B)						
S(1)···H(3B)	H(3B)	0.0240	0.0823	−0.0135	0.0375	*0.0958*
S(1)···H(3C)	H(3C)	0.0909	0.0697	−0.0180	0.1089	*0.0877*
S(1)···H(4B)	H(4B)	0.0342	0.0940	−0.0451	0.0793	*0.1391*
C(1)···H(4C)	H(4C)	0.0014	0.0854	−0.0175	0.0189	*0.1029*

(b) Atomic Potential Energy (PE) of the H Atoms in the Crystal and in the Isolated Ions and Their Corresponding Differences (in au)

		PE (crystal)		PE (isolated)	ΔPE (crystal − isolated)	
interactions	atoms	experiment (E)	theory (T)	DFT	E-DFT	T-DFT
N(1)···H(2)	H(2)	−0.8164	−0.8064	−0.9898	0.1734	*0.1834*
N(1)···H(2B)	H(2B)	−1.2625	−1.2298	−1.2190	−0.0435	*−0.0108*
S(1)···H(2B)						
S(1)···H(3B)	H(3B)	−1.3041	−1.2410	−1.2670	−0.0371	*0.0260*
S(1)···H(3C)	H(3C)	−1.2285	−1.2515	−1.2694	0.0409	*0.0179*
S(1)···H(4B)	H(4B)	−1.3717	−1.2272	−1.2817	−0.0900	*0.0545*
C(1)···H(4C)	H(4C)	−1.3248	−1.2390	−1.2690	−0.0558	*0.0300*

(c) Atomic Dipolar Polarization (M) of the H Atoms in the Crystal and in the Isolated Ions and Their Corresponding Differences (in au)

		M (crystal)		M (isolated)	ΔM (crystal − isolated)	
interactions	atoms	experiment (E)	theory (T)	DFT	E-DFT	T-DFT
N(1)···H(2)	H(2)	0.1407	0.1292	0.1948	−0.0541	*−0.0656*
N(1)···H(2B)	H(2B)	0.1054	0.1072	0.1088	−0.0034	*−0.0016*
S(1)···H(2B)						
S(1)···H(3B)	H(3B)	0.0785	0.1078	0.1314	−0.0529	*−0.0236*
S(1)···H(3C)	H(3C)	0.0689	0.1189	0.1349	−0.0660	*−0.0160*
S(1)···H(4B)	H(4B)	0.0544	0.0894	0.1504	−0.0960	*−0.0610*
C(1)···H(4C)	H(4C)	0.1147	0.0949	0.1348	−0.0210	*−0.0399*

(d) Atomic Volume (V) of the H Atoms in the Crystal and in the Isolated Ions and Their Corresponding Differences (in au)

		V (crystal)		V (isolated)	ΔVT(crystal − isolated)	
interactions	atoms	experiment (E)	theory (T)	DFT	E-DFT	T-DFT
N(1)···H(2)	H(2)	17.31	16.39	34.33	−17.02	*−17.94*
N(1)···H(2B)	H(2B)	40.27	38.87	45.97	−5.70	*−7.10*
S(1)···H(2B)						
S(1)···H(3B)	H(3B)	41.89	41.63	51.25	−9.36	*−9.62*
S(1)···H(3C)	H(3C)	41.32	44.08	50.09	−8.77	*−6.01*
S(1)···H(4B)	H(4B)	43.62	41.16	53.18	−9.56	*−12.02*
C(1)···H(4C)	H(4C)	43.98	41.33	50.04	−6.06	*−8.71*

[a] The symmetry codes are the same as those listed in Table 3.

described by Sorenson et al.[44] in their study on tetrafluoroterephthalotnitrile (TFT). Therefore we conclude that the model with third-order Gram−Charlier coefficients is significantly better in all statistical aspects to the previous model. These striking results prompted us to perform the rest of the calculation with this model. The minimum and the maximum residual density over the entire asymmetric unit, as given in Table 1, confirm the correctness of the model. The almost featureless residual density map (Figure S1), plotted in the plane of the anion and the cation, shows that the residuals, though negligible, are found at the S atom site only. The static deformation density maps (Figure 3) obtained from both the experimental and the theoretical structure factors are in good agreement. The lone pair of electrons on the S atom is prominently seen in both of the maps. Figure 3 also highlights the nature of $N^+-H\cdots N^-$ interaction via deformation maps. The experimental topological parameters of the covalent bonds for the non-hydrogen atoms, along with the values obtained from the periodic theoretical calculations, are given in Table 2. It is noteworthy that the values obtained both from experiment and theory are in good agreement demonstrating that both methodologies provide consistent measures of the topological properties of the charge density. As expected, the location of the BCP for the C−S bond is found to be slightly closer to the S atom while for the C−N bonds it is much closer to the C atoms (Table 2). The highest ($\sim 3e$ Å^{-3}) and lowest ($\sim 1.5e$ Å^{-3}) bonding densities were found at the N(1)−C(1) and S(1)−C(1) bond, respectively.

The calculation of atomic charges via monopole population analysis shows that the charge associated with the anion is $-0.919e$ (theory, $-0.939e$), and the charges on S, C, and N atoms are $-0.399e$ ($-0.315e$), -0.369e ($-0.469e$), and $-0.151e$ ($-0.115e$), respectively. In the cation (total charge, experiment $0.919e$ and theory $0.939e$), all of the C atoms carry positive charges except the N atom (experiment, $-0.266e$ and $-0.349e$), which is bonded to H(2) (experiment 0.360e and theory $0.352e$). All of the H atoms carry positive charges.

The manner in which the ionic species pack in the crystal lattice is determined by the strong as well as weak inter-ion interactions. The details of all the parameters characterizing these interactions, in terms of the first four of the KP criteria, are given in Table 3. At first glance, the crystal contains a single hydrogen-bonded monomer, with the two centrosymmetrically

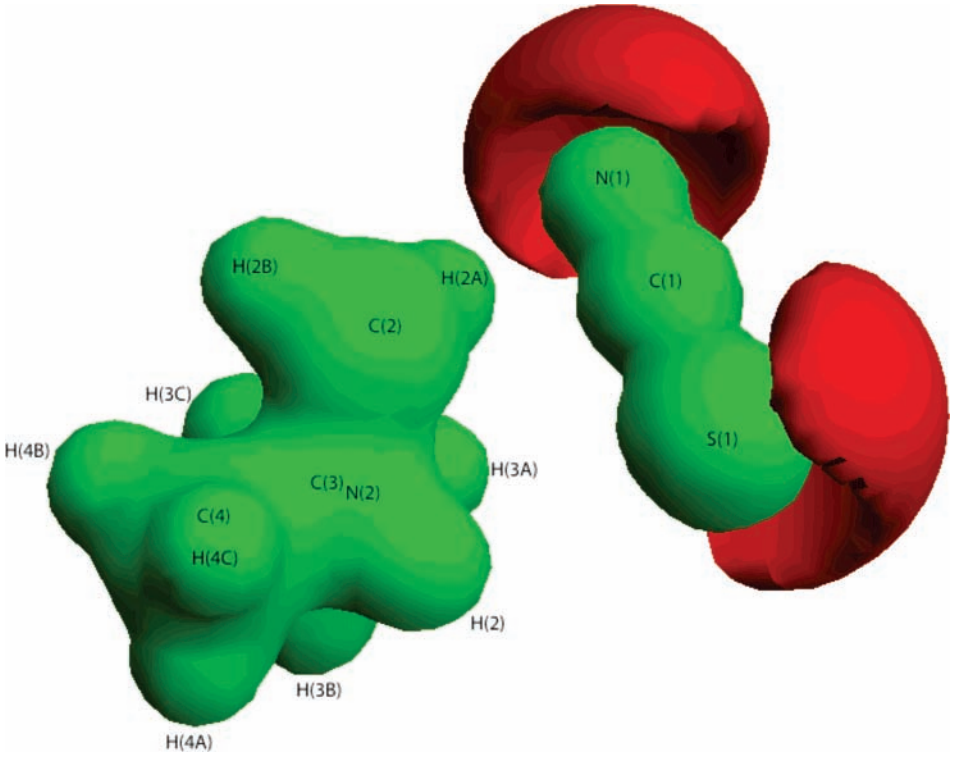

Figure 10. Molecular electrostatic potentials. The potential of $+0.54e$ Å^{-1} is shown as the green isosurface while the potential of $-0.18e$ Å^{-1} is shown as the red isosurface.

related SCN^- anions forming a strong, near-linear $N^+-H\cdots(NCS)^-$ hydrogen bond ($\angle N(2)-H(2)\cdots N(1) = 168.01(2)°$). However, on a more detailed examination, seven other close contacts were observed between the C−H groups of the cation and the atoms of the anion. There are eight unique C−H groups in the cation, H(2A) and H(2B) on the methylene carbon atom, H(3A), etc. on the C(3) methyl group and H(4A), etc. on the second C(4) methyl group. All of the atoms in the anion participate in at least one interaction. In the cation, except for H(2A), H(3A), and H(4A), all of the other five H atoms are involved in interactions. A theoretical/statistical study[45] of hydrogen bonds to the nitrogen and sulfur atoms in the thiocyanate ion found that when there was only one hydrogen bond at the nitrogen atom the X−H···N angle was somewhere in the range of 140−180° with each 10° interval approximately equally populated. If there were more than one hydrogen bond to the nitrogen atom then there was a marked preference for one bond angle to be in the 160−170° range with the second (and subsequent) angles more acute so that the average was 145°. With the hydrogen bond to sulfur the study concluded that there was a preferred interaction with a bond angle of 105° but that a reduction in the electrostatic interactions made an axial approach (180°) also favorable.

In this structure, the strong classical N−H···N hydrogen bond with a bond angle of 168.01(2)°, with the weaker bond at 133.41(1)° [$\angle C(2)-H(2B)\cdots N(1)$] gives a mean of 150.71°. This nicely satisfies the multiple bond criterion of the theoretical/statistical study.[45] For the four interactions to the sulfur atom, three are 127.02(1)° [$\angle C(2)-H(2B)\cdots S(1)$], 134.43(1)° [$\angle C(3)-H(3C)\cdots S(1)$], and 169.27(2)° [$\angle C(4)-H(4B)\cdots S(1)$]. These appear to cluster together (Figure 4) with the bond paths from H(2B) and H(3C) curving inward toward the NCS bond axis. Thus all three interactions approach in one of the two preferred (axial) directions. The interaction from H(3B) however curves slightly away from the NCS bond axis, thus making the approach more acute than the 125.70(2)° [$\angle C(3)-H(3B)\cdots S(1)$] of the direct line. This interaction can be considered as approaching toward the other preferred direction of 105°. Thus even these weak interactions appear to occur within their predicted ranges.

The distributions of the charge density (and its associated parameters) in the inter-ionic spaces provide a quantitative basis for the comparison of the strength of both the strong and the weak interactions. In terms of the characterizing parameters (mainly energy densities), the $N^+-H\cdots N^-$ interaction is found to be the strongest, followed by C−H···S, C−H···N, and C−H···C_π (Table 3). Of the four C−H···S interactions, two show hydrogen bond character while the other two are van der Waals in nature. The C−H···N and C−H···C_π interactions are also found to be van der Waals type, the latter has the smallest value of the electron density and energy densities, hence the weakest interaction. The ionic $N^+-H\cdots N^-$ hydrogen bond is easily distinguishable from the other interactions in terms of the parameters characterizing the interactions (Table 3). Further, in an effort to emphasize these interacting features, the BP characteristics along with the location of (3, −1) BCPs have been highlighted, and the corresponding distributions of the charge densities have been plotted via Laplacian maps from the experimental analysis. The corresponding maps obtained from theoretical analysis show similar features. All of the close contacts were found to possess clear BPs and (3, −1) BCPs. All of the contacts are shown in Figure 4, which highlight the nature of interactions between the cation and the anion. This family of interactions can be divided up into four groups, one ionic $N^+-H\cdots N^-$ (unique), four C−H···S, one C−H···N, and one C−H···C_π. Among these, the S atom alone has four interactions, and the three axial interactions produce a most elegant parasol (Figure 4). Interestingly, all of the interactions are inter-ionic. The nature of the charge density distribution in the region of the strong ionic N^+-H···N^- hydrogen bond is shown in the Laplacian map (Figure 5). The nature of the interactions between the cation, NH^+, and the anion, SCN^-, is

clearly seen in this map. The Laplacian map in Figure 6 shows the distribution of charges in the region of the bifurcated C−H···S interactions, at the S atom, which participates in four such interactions. The Laplacian distribution of the other C−H···S interaction generated from H(3B) is shown in Figure 7. The bifurcated C−H···S and C−H···N interactions, at H(2B), are shown via the Laplacian map in Figure 8. The only C−H···C_π interaction, generated from the anion SCN^-, indicates that it is directed toward the C−N bond rather than the C atom alone (Figure 9). Figure 9 also illustrates the features associated with the Laplacian distribution of the atoms in the SCN^- anion. These maps show the nature of the interacting features and hence the electron density distribution between the cationic C−H and N−H groups and the anion. It is interesting to note that the charge density features associated with these inter-ion interactions are similar to those in molecular crystals, and these are expected to follow a similar pattern, as reported in earlier studies.[5,6,33,46] On inspection of the parameters listed in the Table 3 it is clear that the topological properties, such as electron density, Laplacian, local kinetic, and potential energy densities, and interpenetration of van der Waals spheres correlate well with the length of the interactions.[46]

Criteria 5−8 deal with the evaluation of integrated properties over the basin of the H atoms participating in the interactions. These properties are calculated for both the crystal (experimental and theoretical) and the isolated ions in the gas phase. The components forming the basis of criteria 5−8 are given in Tables 4a−d. Since the integrated properties of the isolated ions can only be obtained from theoretical calculation, the results from the theoretical calculations that took into account the periodicity of the crystal (values given in italics in Table 4) appear the most reliable, and the discussions are limited to these values. The increment of the atomic net charges, Δq, (Table 4a) of the H atoms participating in the interactions shows the expected trend, and it is higher for the strong hydrogen bonds when compared with the weaker interactions.[33,42] From the theoretical calculations the highest increment (0.1398 au) was found at the H(2) atom of the N^+−H···N^- hydrogen bond, while the lowest (0.0591 au) was for interactions at the H(2B) atom on the methylene carbon. A similar trend is observed in the increment of the potential energy (PE), with the highest value of 0.1834 au and the lowest value of −0.0108 au located at the same atoms (Table 4b). Again, the difference in values of the dipolar polarization (ΔM) has the highest magnitude (0.0656 au) at the H(2) atom (Table 4c), and the lowest magnitude (0.0016 au) is at H(2B). The depletion of the atomic volumes follows the expected trend: The H(2) atom with strongest hydrogen bond shows largest depletion (−17.94 au) while H(3C) shows the least (−6.01 au) and H(2B) shows the second lowest (−7.10 au) depletion (Table 4d). In general, all of the properties derived from theory show the expected trends for the formation of a hydrogen bond or van der Waals interaction.[33,42]

The electrostatic potential (ESP) maps have been derived from experimental charge densities; the corresponding maps from the theoretical analysis also reveal similar features. The construction of a three-dimensional ESP map plotted over the ionic surfaces (Figure 10) clearly emphasizes the ionic character of the compound. It is to be noted that the large electropositive surface at the cation is well-separated from that of the anion. However, as expected, the maximum spread of the electronegative surface is seen at the anion SCN^-, which consists of all of the acceptors responsible for the inter-ionic interactions. The preferred binding sites to form the network of interactions available in the structure are prominent from this map (Figure 10).

Concluding Remarks

This is the first example of an inter-ion interaction where the whole range from classical hydrogen bond to weak van der Waals is present in the interaction, and they can thus be compared. This is also the first full examination of the SCN^- anion since the charge density study of NaSCN and NH_4SCN nearly 30 years ago.[2,3] In this anion, the S atom is best treated by the default deformation density exponents, but the thermal motion needs refining with third-order coefficients of a Gram−Charlier expansion. Even in this simplest of systems, the picture of the interactions between the ions is quite intricate. However, using the criteria proposed by Koch and Popelier it is now possible to understand the nature of the intra/intermolecular interactions involved in this complex. It can be shown that the N(1)···H(2), S(1)···H(3B), and S(1)···H(3C) interactions can be classified as hydrogen bonds. The strong N(1)···H(2) hydrogen bond being somewhat covalent in nature, whereas the weaker S···H hydogen bonds are predominantly closed-shelled in nature. The other interactions are best classified as weak van der Waals interactions and even though they cannot be classified as hydrogen bonds, it can be shown that they play an important role in directing the packing of this complex and thus play a crucial role in the crystalline stability of the complex.

Acknowledgment. P.M. thanks the Council of Scientific and Industrial Research, India, for a senior research fellowship. E.C. and T.S.C. acknowledge the support of National Sciences and Engineering Research Council of Canada and Dalhousie University. P.M., T.N.G., E.C., and T.S.C. gratefully acknowledge all of the help and assistance at RigakuMSC in collecting the X-ray diffraction data. We thank the reviewers for their valuable comments and suggestions and especially to one of the reviewers for the clarification of thermal motion analysis on S atom.

Supporting Information Available: The Supporting Information contains (i) residual density maps and (ii) the crystallographic information files. This material is available free of charge via the Internet at http://pubs.acs.org.

References and Notes

(1) Macchi, P.; Iversen, B. B.; Sironi, A.; Chakoumakos, B. C.; Larsen F. K. *Angew. Chem., Int. Ed.* **2000**, *39*, 2719−2722.

(2) Bats, J. W.; Coppens, P.; Kvick, Å. *Acta Crystallogr., Sect. B* **1977**, *33*, 1534−1542.

(3) Bats, J. W.; Coppens, P. *Acta Crystallogr., Sect. B* **1977**, *33*, 1542−1548.

(4) Abramov, Yu. A. *J. Phys. Chem. A* **1997**, *101*, 5725−5728.

(5) Mallinson, P. R.; Smith, G. T.; Wilson, C. C.; Grech, E.; Wozniak, K. *J. Am. Chem. Soc.* **2003**, *125*, 4259−4270.

(6) Wolstenholme, D; Aquino M. A. S.; Cameron, T. S.; Ferrara, J. D.; Robertson, K. N. *Can. J. Chem.* **2006**, *84*, 804−811.

(7) Amendola, V.; Boiocchi, M.; Fabbrizzi, L.; Palchetti, A. *Chem.−Eur. J.* **2005**, *11*, 120−127.

(8) (a) Coppens, P. *X-ray Charge Densities and Chemical Bonding*; Oxford University Press: Oxford, U. K., 1997. (b) Spackman, M. A. *Annu. Rep. Prog. Chem., Sect. C: Phys. Chem.* **1997**, *94*, 177−207. (c) Koritsanszky, T. S.; Coppens, P.; *Chem. Rev.* **2001**, *101*, 1583−1621. (d) Reference 8a, p 136.

(9) Desiraju, G. R. *Crystal Engineering: The Design of Organic Solids*; Elsevier: Amsterdam, 1989.

(10) (a) Stewart, R. F.; Craven, B. M. *Biophys. J.* **1993**, *65*, 998−1005. (b) Spackman, M. A.; Byrom, P. G. *Acta Crystallogr., Sect. B* **1996**, *52*, 1023−1035.

(11) Coppens, P. *Acta Crystallogr., Sect. A* **1998**, *54*, 779−788.

(12) Lecomte, C. In *Advances in Molecular Structure Research*; Hargittai, I., Hargittai, M., Eds.; JAI Press: Greenwich, CT, 1995; pp 261−302.

(13) Hansen, N. K.; Coppens, P. *Acta Crystallogr., Sect. A* **1978**, *34*, 909−921.

(14) (a) Bader, R. F. W. *Atoms in Molecules: A Quantum Theory*; Clarendon Press, Oxford, U. K., 1990. (b) Bader. R. F. W. *J. Phys. Chem. A* **1998**, *102*, 7314−7323.
(15) Popelier, P. L. A. *Atoms in Molecules: An Introduction*; Prentice Hall: New York, 2000; pp 150−153.
(16) Koch, U.; Popelier, P. L. A. *J. Phys. Chem.* **1995**, *99*, 9747−9754.
(17) (a) Abramov, Yu. A. *Acta Crystallogr.. Sect. A* **1997**, *53*, 264−272. (b) Espinosa, E.; Molins, E.; Lecomte, C. *Chem. Phys. Lett.* **1998**, *285*, 170−173.
(18) (a) Bondi, A. *J. Phys. Chem.* **1964**, *68*, 441−451. (b) Nyburg, S. C.; Faerman, C. H. *Acta, Crystallogr., Sect. B* **1985**, *41*, 274−279.
(19) Cameron, E. The Hydrogen Bonding of $Zn(SCN)_2L$ where L = $Me_xH_{2-x}N(CH_2)_2NH_{2-y}Me_y$, $x,y \leq 2$ and the Hydrogen Bonding of Organo-Ammonium Thiocyanates. M.Sc. Thesis, Dalhousie University 1998.
(20) Otwinowski, Z.; Minor W. Processing of X-ray diffraction data collected in oscillation mode; In *Macromolecular Crystallography, Part A*; Carter, C. W., Jr., Sweet, R. M., Eds.; Methods in Enzymology 276; Academic Press: New York, 1997; pp 307−326.
(21) Blessing, R. H. *Crystallogr. Rev.* **1987**, *1*, 3−58.
(22) Sheldrick, G. M. *SHELXS97* and *SHELXL97*; University of Göttingen: Göttingen, Germany, 1997.
(23) Farrugia, L. J. WinGX, version 1.64.05. *J. Appl. Crystallogr.* **1999**, *32*, 837−838.
(24) Farrugia, L. J. ORTEP-3. *J. Appl. Crystallogr.* **1997**, *30*, 565.
(25) Johnson, C. K. *ORTEP*; Report ORNL-3794; Oak Ridge National Laboratory: Oak Ridge, TN, 1965.
(26) Koritsanszky, T. S.; Howard, S.; Macchi, P.; Gatti, C.; Farrugia, L. J.; Mallinson, P. R.; Volkov, A.; Su, Z.; Richter, T.; Hansen, N. K. *XD, A Computer Program Package for Multipole Refinement and Analysis of Electron Densities from Diffraction Data*, version 4.10; Free University of Berlin: Berlin; University of Wales: Cardiff, U. K.; Università di Milano: Milano, Italy; University of Glasgow: Glasgow, U. K.; State University of New York: Buffalo, NY; University of Nancy: Nancy, France, 2003.
(27) Clementi, E.; Roetti, C. *At. Data Nucl. Data Tables.* **1974**, *14*, 177−478.
(28) Allen, F. H. *Acta Crystallogr., Sect. B* **1986**, *42*, 515−522.
(29) Abramov, Yu. A.; Volkov, A.; Coppens, P. *Chem. Phys. Lett.* **1999**, *311*, 81−86.
(30) Saunders, V. R.; Dovesi, R.; Roetti, C.; Orlando, R.; Zicovich-Wilson, C. M.; Harrison, N. M.; Doll, K.; Civalleri, B.; Bush, I.; D'Arco, Ph.; Llunell, M. *CRYSTAL2003 User's Manual*; University of Torino: Torino, Italy, 2003.
(31) (a) Becke, A. D. *J. Chem. Phys.* **1993**, *98*, 5648−5652. (b) Lee, C.; Yang, W.; Parr, R. G. *Phys. Rev. B* **1988**, *37*, 785−789.
(32) Hariharan, P. C.; Pople, J. A. *Theor. Chim. Acta* **1973**, *28*, 213−222.
(33) Munshi, P.; Guru Row, T. N. *J. Phys. Chem. A* **2005**, *109*, 659−672.
(34) Oddershede, J.; Larsen; S. *J. Phys. Chem. A* **2004**, *108*, 1057−1063.
(35) Volkov, A.; Gatti, C.; Abramov, Yu.; Coppens, P. *Acta Crystallogr., Sect. A* **2002**, *56*, 252−258.
(36) Popelier, P. L. A. with a contribution from Bone, R. G. A .*MORPHY98*; UMIST: Manchester, U. K., 1998.
(37) Frisch, M. J.; Trucks, G. W.; Schlegel, H. B.; Scuseria, G. E.; Robb, M. A.; Cheeseman, J. R.; Zakrzewski, V. G.; Montgomery, J. A., Jr.; Stratmann, R. E.; Burant, J. C.; Dapprich, S.; Millam, J. M.; Daniels, A. D.; Kudin, K. N.; Strain, M. C.; Farkas, O.; Tomasi, J.; Barone, V.; Cossi, M.; Cammi, R.; Mennucci, B.; Pomelli, C.; Adamo, C.; Clifford, S.; Ochterski, J.; Petersson, G. A.; Ayala, P. Y.; Cui, Q.; Morokuma, K.; Malick, D. K.; Rabuck, A. D.; Raghavachari, K.; Foresman, J. B.; Cioslowski, J.; Ortiz, J. V.; Stefanov, B. B.; Liu, G.; Liashenko, A.; Piskorz, P.; Komaromi, I.; Gomperts, R.; Martin, R. L.; Fox, D. J.; Keith, T.; Al-Laham, M. A.; Peng, C. Y.; Nanayakkara, A.; Gonzalez, C.; Challacombe, M.; Gill, P. M. W.; Johnson, B. G.; Chen, W.; Wong, M. W.; Andres, J. L.; Head-Gordon, M.; Replogle, E. S.; Pople, J. A. *Gaussian 98*; Gaussian, Inc.: Pittsburgh, PA, 1998.
(38) Hirshfeld, F. L. *Acta Crystallogr., Sect. A* **1976**, *32*, 239−244.
(39) Dominiak, P. M.; Coppens, P. *Acta Crystallogr., Sect. A* **2006**, *62*, 224−227.
(40) For a discussion of these values (exponents), see ref 8a, pp 65−67.
(41) Overgaard, J.; Hibbs, D. E. *Acta Crystallogr., Sect. A* **2004**, *60*, 480−487.
(42) Munshi, P.; Thakur T. S.; Guru Row, T. N.; Desiraju, G. R. *Acta Crystallogr., Sect. B* **2006**, *62*, 118−127.
(43) Munshi, P.; Guru Row, T. N. *Acta Crystallogr., Sect. B* **2006**, *62*, 612−626.
(44) Sorensen, H. O.; Stewart, R. F.; McIntyre, G. J.; Larsen, S. *Acta Crystallogr., Sect. A* **2003**, *59*, 540.
(45) Lommerse, J. P. M.; Cole, J. C. *Acta Crystallogr., Sect. B* **1998**, *54*, 316−319.
(46) Munshi, P.; Guru Row, T. N. *CrystEngComm* **2005**, *7*, 608−611.